

Redox equilibria of iron in alkaline earth silicate melts: relationships between melt structure, oxygen fugacity, temperature and properties of iron-bearing silicate liquids

BJØRN O. MYSEN, DAVID VIRGO AND FRIEDRICH A. SEIFERT¹

*Geophysical Laboratory, Carnegie Institution of Washington
Washington, D. C. 20008*

Abstract

Mössbauer and Raman spectroscopy have been used to relate redox equilibria of iron to melt structure in MO–SiO₂ systems (M = Ba²⁺, Sr²⁺, Ca²⁺, Mg²⁺). Log Fe²⁺/Fe³⁺ is a linear function of log *f*_{O₂}, although the slope of the lines depends on bulk composition. The Fe²⁺/Fe³⁺ is a linear function of NBO/T (nonbridging oxygens per tetrahedral cation) for each type of divalent metal cation. The ferrous–ferric ratio is also proportional to *Z/r*² of the metal cation at constant M/Si (or NBO/Si) of the melts.

With Fe²⁺/Fe³⁺ < 1, ferric iron is in tetrahedral coordination. The spectroscopic data indicate that further reduction may result in a coordination transformation of the remaining Fe³⁺, probably to six-fold coordination. The Fe²⁺/Fe³⁺ of this transformation appears insensitive to the type of metal cation and the NBO/T of the melt. Its value increases somewhat as the total iron content of the system is increased.

Liquidus phase equilibria for compositions with Ca/Si = 0.7 and Mg/Si = 0.7, with 10 wt.% iron oxide added were calculated as a function of Fe²⁺/Fe³⁺. An increase in Fe²⁺/Fe³⁺ results in a decrease of 35°C in the liquidus temperature in the system CaO–SiO₂–Fe₂O₃–FeO (at Fe²⁺/Fe³⁺ ~ 0.25). In the analogous Mg-bearing system, the maximum temperature decrease is 200°C (at Fe²⁺/Fe³⁺ ~ 4.0). Silica polymorphs (and, over a limited ferric/ferrous range, two liquids in the Mg-bearing system) occur on the liquidus until the temperature minimum is reached. With additional increase in Fe²⁺/Fe³⁺, metasilicate minerals (pseudowollastonite and clinoenstatite, respectively) are stable. In the system MgO–SiO₂–Fe₂O₃–FeO, a silica polymorph (cristobalite) reappears on the liquidus with Fe²⁺/Fe³⁺ ~ 9.0, whereas in the analogous Ca system, pseudowollastonite remains on the liquidus until all ferric iron has been reduced to ferrous iron.

Introduction

Iron oxide redox equilibria in magmatic liquids are of interest because Fe²⁺/Fe³⁺ influences melt structure and derivative properties (Mysen et al., 1982b) and because the distribution of iron oxides between liquidus minerals and melt may be used as an indicator of magmatic history (e.g., Bowen et al., 1930; Mysen et al., 1980; Haggerty, 1978; Sato and Valenza, 1980). Preliminary data indicate that ferric iron may be both a network former and a network modifier (e.g., Mysen et al., 1980), whereas ferrous iron commonly is considered to be a network modifier in silicate melts (e.g., Mao et al., 1973; Nolet et al., 1979). Thus melt properties that depend on melt polymerization may also depend on iron content and Fe³⁺/ΣFe.

The redox ratio of iron oxides and the structural position of Fe³⁺ and Fe²⁺ in melts may depend on the

type of metal cations available for charge-balance of Fe³⁺ in tetrahedral coordination and the proportions of coexisting anionic units (Dickinson and Hess, 1981; Mysen et al., 1982b). These proportions are related to the network-modifying cations in the melts (Mysen et al., 1982b). In natural magmatic liquids, alkaline earths commonly are the most abundant network-modifying cations and may also potentially serve to charge-balance Fe³⁺ in tetrahedral coordination in analogy with observations on alkaline-earth-bearing aluminosilicate systems (e.g., Seifert et al., 1982; Navrotsky et al., 1982). In order to describe the interrelations between redox equilibria of iron oxides and the structure of magmatic liquids, we decided, therefore, to study the effect of temperature and oxygen fugacity on the redox equilibria of iron oxide in simple alkaline earth silicate melts.

Experimental methods

Starting materials were spectroscopically pure (Johnson and Matthey) SiO₂, CaCO₃, BaCO₃, SrCO₃, MgO and Fe₂O₃. Approximately 10% of the Fe₂O₃ was added as isotopically enriched

¹ Present address: Mineralogisch-Petrographisches Institut und Museum, Universität Kiel, 2300-Kiel, West Germany.

⁵⁷Fe₂O₃ (90–95% ⁵⁷Fe) to enhance the sensitivity of Mössbauer spectra for the determination of Fe²⁺/Fe³⁺ and the structural positions of Fe²⁺ and Fe³⁺. Batches of 200–300 mg were ground under alcohol for 1 hr or more, dried at 400°C and stored at 110°C until used. The samples (30–70 mg) were suspended on 0.1-mm Pt loops (Presnall and Brenner, 1974) in vertical Pt- and MoSi₂-heated, quench furnaces. All samples were quenched in either liquid nitrogen or water. The oxygen fugacity in the furnace was controlled with CO–CO₂ gas mixing and monitored with an Y₂O₃-doped ZrO₂ oxygen sensor (Sato, 1972). The accuracy of the sensor was checked periodically against the equilibria 2Ni + O₂ ⇌ 2NiO and 2Fe + O₂ ⇌ 2FeO (Chou, 1978; Deines et al., 1974). The accuracy of the oxygen fugacity, based on this calibration, is better than 0.1 log unit of *f*_{O₂} at the temperature of these experiments (1550°C). The precision is 0.01–0.02 log unit. The composition of the glasses, within analytical uncertainty (2%, relative), accords with the nominal values. Electron microprobe analyses are available from the authors upon request. The compositions of the starting materials, as used throughout this report, are defined with their symbols as described in Table 1.

Raman and Mössbauer spectra were obtained with the auto-

mated Raman and Mössbauer systems at the Geophysical Laboratory (e.g., Mysen et al., 1982a). The Raman data were obtained by excitation of the sample with the 514-nm line of an Ar⁺-ion laser with 2–4 watts at the sample with the same configurations as in Seifert et al. (1982). The samples were examined optically before and after exposure to the laser to evaluate possible radiation damage. On occasion, discoloration and sometimes precipitation of an iron oxide were observed. In such cases, the Raman spectrum was discarded. Mössbauer spectra were obtained on the same samples, occasionally both before and after exposure to the laser beam. In optically clear glasses, no effects of laser exposure could be observed in the Mössbauer spectra. All other aspects of the Raman methods have been described elsewhere (Mysen et al., 1982a; Virgo et al., 1981, 1982; Seifert et al., 1982). Curves of Lorentzian and Gaussian line shapes were fitted to the digitized output from the Mössbauer and Raman spectrometers, respectively, as summarized elsewhere (Mysen and Virgo, 1978; Virgo et al., 1981, 1982, 1983a; Mysen et al., 1980, 1982a).

Alternative fitting methods of the Mössbauer spectra with different lines-shapes (e.g., Eibschutz, et al., 1980; Eibschutz and Lines, 1982), or with least-squares fitting of an assumed correlation of hyperfine parameters of a large number of elementary doublets (e.g., Wivel and Morup, 1981) were attempted. These methods did not yield results for Fe³⁺/ΣFe or hyperfine

² It is recalled that Fe³⁺/ΣFe, obtained directly from the Mossbauer spectra, is related to Fe²⁺/Fe³⁺ as Fe²⁺/Fe³⁺ = (1 – Fe³⁺/ΣFe)/(Fe³⁺/ΣFe).

Table 1. Mössbauer results

Composition	Temp., °C	-log <i>f</i> _{O₂}	Fe ³⁺		Fe ²⁺ (I)		Fe ²⁺ (II)		Fe ³⁺ /ΣFe
			IS*	QS*	IS	QS	IS	QS	
CS2F2.3	1725	0.68	0.70	0.71	1.05	2.19	0.85	1.87	0.249
CS2F4.6	1725	0.68	0.56	0.78	1.01	2.26	0.85	1.93	0.396
CS2F9.1	1725	0.68	0.31	1.17	1.10	2.02	0.92	1.65	0.443
CS2F5	1550	0.68	0.32	1.17	1.08	2.02	0.91	1.67	0.584
CS2F5	1550	2.50	0.53	0.85	1.07	2.16	0.93	1.88	0.247
CS1.4F5	1550	0.68	0.32	1.13	1.11	2.10	0.95	1.78	0.614
CS1.4F5	1550	2.50	0.57	0.77	1.07	2.18	0.92	1.89	0.288
CS1.4F5	1550	4.00	0.57	0.55	1.05	2.03	0.86	1.65	0.117
CS1.4F5	1550	6.00	1.04	2.21	1.01	1.65	0.000
CS1.2F5	1550	0.68	0.32	1.14	1.06	2.05	0.91	1.76	0.638
CS1.2F5	1550	2.50	0.52	0.79	0.96	2.27	0.75	1.68	0.356
CSF5	1550	0.68	0.31	1.15	1.11	2.15	0.96	1.85	0.675
CSF5	1550	2.50	0.46	0.91	1.05	2.20	0.89	1.88	0.417
CSF5	1550	4.00	0.55	0.69	1.00	2.29	0.97	1.71	0.228
CS.8F5	1550	0.68	0.32	1.19	1.00	1.99	0.710
CS.8F5	1550	2.50	0.34	1.16	1.08	2.12	0.91	1.77	0.472
CS.7F5	1550	0.68	0.32	1.20	1.00	2.08	0.823
CS1.4F10	1550	0.68	0.32	1.16	1.00	2.00	0.677
CS1.4F10	1550	2.50	0.33	1.12	1.11	2.05	0.95	1.75	0.397
CS1.4F10	1550	4.00	0.55	0.71	1.11	2.06	0.95	1.91	0.231
MS1.4F5	1550	0.68	0.34	1.24	1.15	2.13	0.99	1.81	0.523
MS1.4F5	1550	2.50	0.70	0.77	1.12	2.21	0.95	1.86	0.188
MS1.4F5	1550	4.00	0.85	1.02	1.13	2.14	0.96	1.80	0.065
MS1.4F5	1550	6.00	1.05	2.18	0.92	1.52	0.000
MS1.2F5	1550	0.68	0.37	1.33	1.16	2.10	1.00	1.77	0.482
MS1.2F5	1550	2.50	0.70	0.90	1.11	2.19	0.95	1.89	0.222
SrSF5	1550	0.68	0.30	1.09	1.00	1.82	0.746
BS4F5	1550	0.68	0.30	0.97	0.94	2.00	0.684
BS3F5	1550	0.68	0.30	0.98	0.95	1.96	0.684
BS2F5	1550	0.68	0.29	0.97	0.97	1.97	0.699
BS1.5F5	1550	0.68	0.29	0.96	0.95	1.93	0.731
BS1.2F5	1550	0.68	0.27	0.96	0.95	1.91	0.771
BS1.1F5	1550	0.68	0.28	0.97	0.93	1.93	0.784
BSF5	1550	0.68	0.29	0.90	0.75	2.18	0.833

*Isomer shift (IS) and quadrupole splitting (QS) (mm/sec) relative to Fe metal.

Abbreviations: C, CaO; M, MgO; Sr, SrO; B, BaO; S, SiO₂; F, Fe₂O₃. CS2, etc., refer to molar SiO₂/metal oxide. CS2F5, etc., refer to wt.% Fe₂O₃ added to starting material.

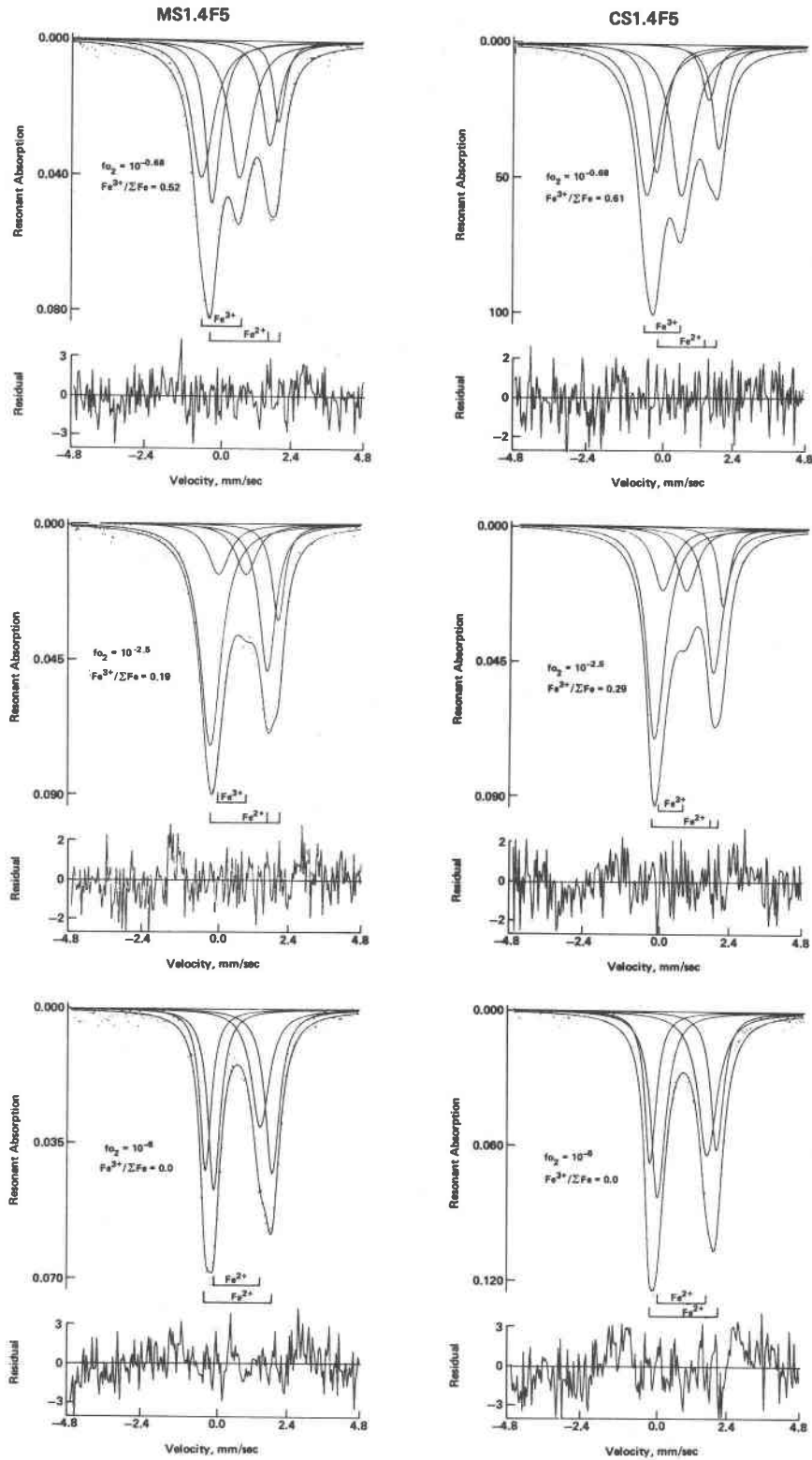


Fig. 1. Comparison of Mössbauer spectra of melts (obtained at 298 K) with composition CS1.4F5 ($SiO_2/CaO = 1.4$, with 5 wt.% Fe_2O_3 added) and MS1.4F5 ($SiO_2/MgO = 1.4$, with 5 wt.% Fe_2O_3 added) at 1550°C as a function of oxygen fugacity.

parameters that were significantly different from those reported here. Thus, the fitting methods employed in earlier reports (e.g., Virgo et al., 1981, 1982, 1983a) were employed. In these fits, the areas of the individual doublets were constrained to be equal, as well as the line-width of the ferric doublets. The latter constraint was not imposed on the Fe²⁺-doublet(s) as Mössbauer spectra for highly reduced glasses typically indicate that Fe²⁺-doublets are asymmetric (e.g., Mao et al., 1973; Mysen and Virgo, 1978; Nolet et al., 1979; Levitz et al., 1980). In the most oxidized samples, the spectra can be resolved into one ferric doublet and two high-velocity components of two Fe²⁺ doublets. The two corresponding low-velocity components nearly coincide and could not be resolved statistically. With the resultant five-line fit (without the area constraints for the Fe²⁺ components), the area of the single Fe²⁺-low velocity component is similar to the sum of the two high-velocity components within 5% relative. In reduced samples two asymmetric ferrous doublets result in the statistically best fit (e.g., Fig. 1). These two Fe²⁺-doublets are denoted Fe²⁺(I) and Fe²⁺(II) in the text. Interested readers may contact the authors for additional details and program listings for the alternative and current fitting routines.

Results

Mössbauer data

Relationships between Mössbauer data and bulk melt composition, temperature and oxygen fugacity are summarized in Table 1 with selected Mössbauer spectra in Figure 1. Decreasing *f*_{O₂} results in a rapid decrease in the intensity of the resonant absorption between 0.5 and 0.8 mm/sec in the Mössbauer spectra and a slight shift to higher velocity of the high-velocity component of the ferric doublet (Fig. 1). This spectroscopic change is associated with an increase in absorption in the highest- and lowest-velocity portions of the spectra. These spectroscopic features result from the increase in Fe²⁺/Fe³⁺ of the melts and a slight increase in the velocity of the low-velocity component of the Fe³⁺ doublet.

At the same oxygen fugacity, temperature and degree of polymerization of the melt, the Fe²⁺/Fe³⁺ increases in the order Ba²⁺ < Sr²⁺ < Ca²⁺ < Mg²⁺ (*Z/r*² increases) (Fig. 2), as also observed by Douglas et al. (1965), Lauer and Morris (1977) and Mysen et al. (1980). The Fe²⁺/Fe³⁺ is linearly correlated with the degree of polymerization of the melt (NBO/T) at the same temperature and *f*_{O₂} (Fig. 3). The dependence of Fe²⁺/Fe³⁺ on NBO/T³ (or NBO/Si)

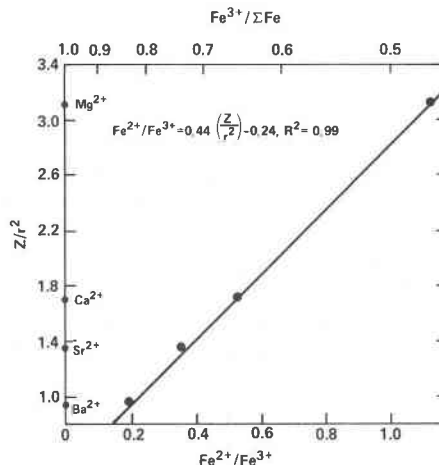


Fig. 2. Relationship between Fe²⁺/Fe³⁺ and type of metal cation (Ba²⁺, Sr²⁺, Ca²⁺, Mg²⁺), expressed as *Z/r*² (*Z* = electrical charge, *r* = ionic radius for six-fold coordination; Whittaker and Muntus, 1970) for metasilicate melt compositions equilibrated at 1550°C in air.

is also a function of the type of network-modifying cation, the oxygen fugacity and the anionic structure of the melt (Table 2; Figs. 1 and 3). The slopes of the lines increase as the metal cation is changed from Ca²⁺ to Ba²⁺, and for the same metal cation, with decreasing *f*_{O₂} (Fig. 3).

As is commonly observed in silicate systems (e.g., Fudali, 1965; Lauer and Morris, 1977; Mysen et al., 1980; Goldman, 1983), there is a nearly linear relationship between log *f*_{O₂} and log (Fe²⁺/Fe³⁺) (Fig. 4). The slope of the lines decreases, however, from about -0.4 for the calcium disilicate composition to about -0.25 as the NBO/T of the melt increases toward that of calcium metasilicate (Fig. 4). The slope is also greater for Mg-bearing systems than for Ca-bearing systems and may decrease (in an absolute sense) with increasing iron content of the system (Fig. 4). This behavior differs from that of Fe²⁺/Fe³⁺ in alkali silicate systems, where the slope does not deviate significantly from -0.25 (Mysen et al., 1980; Virgo et al., 1983a). Thus, the activity coefficient ratio, γFe³⁺/γFe²⁺, decreases with increasing NBO/T and with decreasing *Z/r*² of metal cations in alkaline earth silicate melts, whereas this ratio is independent of NBO/T in alkali silicate systems.

Regardless of the degree of polymerization of the silicate solvent (expressed as NBO/Si), the IS_{Fe³⁺} remains at about 0.3 mm/sec until Fe³⁺/ΣFe decreases below 0.5 (Fig. 5). With Fe³⁺/ΣFe between 0.5 and 0.4, the IS_{Fe³⁺} and QS_{Fe³⁺} change rapidly as a function of decreasing

³ The NBO/T may be calculated from bulk chemical composition after recasting to chemical formula and assignment of tetrahedrally coordinated cations (from structure determinations). Two equivalent expressions,

$$NBO/T = 1/T \sum_{i=1}^i 1/nM_i^{n+}$$

or NBO/T = (2O - 4T)/T, can be used. In these expressions *n* is the electrical charge of network-modifying cations M_{*i*}, *T* is the total number of tetrahedrally coordinated cations and *O* is the number of oxygens. Metal cations required for charge-balance of tetrahedral cations such as Al³⁺ and Fe³⁺ are subtracted from

their total abundance to obtain M_{*i*}. In this paper, the NBO/T and NBO/Si are used as expressions indicating structural and compositional features of the melts in the sense that, if the tetrahedrally coordinated cations are known, the value of NBO/T can be calculated from bulk composition.

Table 2. Average values of hyperfine parameters* (relative to Fe metal)

System	Fe ³⁺		Fe ²⁺ (I)		Fe ²⁺ (II)	
	IS	QS	IS	QS	IS	QS
CaO-SiO ₂ Fe ³⁺ (IV)†	0.318 ± 0.004	1.16 ± 0.03	1.06 ± 0.05	2.06 ± 0.06	0.93 ± 0.02	1.74 ± 0.08
CaO-SiO ₂ Fe ³⁺ (VI)	0.57 ± 0.06	0.73 ± 0.09	1.04 ± 0.05	0.90 ± 0.11	1.82 ± 0.11	
MgO-SiO ₂ Fe ³⁺ (IV)	0.35 ± 0.02	1.32 ± 0.07	1.19 ± 0.06	2.18 ± 0.12	1.01 ± 0.02	1.82 ± 0.06
MgO-SiO ₂ Fe ³⁺ (VI)	0.70 ± 0.00	0.84 ± 0.09	1.12 ± 0.01	2.20 ± 0.01	0.94 ± 0.02	1.88 ± 0.02
SrO-SiO ₂ Fe ³⁺ (IV)	0.30	1.09	1.00	1.82		
BaO-SiO ₂ Fe ³⁺ (IV)	0.29 ± 0.01	0.96 ± 0.03	0.92 ± 0.08	1.98 ± 0.09		

*Isomer shift (IS) and quadrupole splitting (QS) in mm/sec.
†(IV) and (VI) refer to inferred coordination of Fe³⁺.

redox ratio (oxygen fugacity). This ferric/ferrous range is insensitive to the type of metal cation (Fig. 5; see also Virgo et al., 1983a, for data on alkali and alkaline earth aluminosilicate systems). It is noted, however, that in CS1.4 melt (NBO/Si of calcium silicate solvent equals 1.4) the change in IS_{Fe³⁺} and QS_{Fe³⁺} occurs at somewhat lower values of Fe³⁺/ΣFe for 10 wt.% than for 5 wt.% Fe₂O₃ added (cf. CS1.4F5 and CS1.4F10, Fig. 5).

Raman data

Raman spectra were obtained on three compositions with NBO/Si of the iron-free end-member composition equal to 1 (CS2), 1.4 (CS1.4) and 2.38 (CS.8). The spectra of the end members and other relevant compositions have been reported and interpreted elsewhere (Verweij, 1979a, b; Verweij and Konijnendik, 1976; Brawer and White, 1977; Furukawa et al., 1981; Virgo et al., 1980; Mysen et al., 1982b; Domine and Periou, 1983) and only one example is included here for reference (Fig. 6).

The spectra are interpreted on the basis (see Mysen et al., 1982b; Domine and Piriou, 1983, for reviews; and Furukawa et al., 1981, for theoretical calculations) that the anionic structure of melts on binary metal oxide silicate joins may be described as combinations of structural units with NBO/Si values corresponding to the stoichiometric expressions, SiO₄⁴⁻, Si₂O₆⁶⁻, SiO₃²⁻, Si₂O₅³⁻ and SiO₂. For the compositions in the present study, the assignments of the most important Raman bands associated with the various structural units are summarized in Table 3.

For quenched melts equilibrated in air, a distinct difference between the spectra of iron-bearing and iron-free samples is the depolarized band near 990 cm⁻¹ in the spectrum of CS2F5. For this melt, as well as those of CS1.4F5 and CS.8F5, there is also an increase in Raman scattering intensity near 900 cm⁻¹ (Table 3). Furthermore, the relative intensity of the band near 1100 cm⁻¹ in CS2F5 and CS1.4F5 melts (assigned to Si-O⁻ stretch vibrations in Si₂O₅³⁻ units) is lowered as Fe₂O₃ is added to the melt and equilibrated with air at 1550°C. There may be a slight relative increase in intensity near 1150 cm⁻¹ (Si-O^o stretching in three-dimensional network units) and a

more pronounced relative increase in the 950-cm⁻¹ band (Si-O⁻ stretching in SiO₃²⁻ units; Furukawa et al., 1981). The addition of 10 wt.% Fe₂O₃ to CS1.4 melts results in further evolution of these trends (Table 3). Also, the asymmetry of the band near 600 cm⁻¹ (mixed stretch and bending mode of Si-O-Si bridging bonds in depolymerized structural units) becomes very pronounced. At oxygen fugacity below about 10^{-2.5} (and decreasing Fe³⁺/ΣFe), melts of composition CS1.4F5 (Fig. 6) have Raman spectra with only those bands observed in the iron-free system. The intensities of the bands (Table 3), in particular the ratio between the 1100- and 950-cm⁻¹ bands, have changed, however, relative to those of iron-free CaO-SiO₂ melts with similar NBO/Si (Fig. 6; see also Fig. 3 in Mysen et al., 1982b).

Structural interpretation

The 900- and 990-cm⁻¹ bands in the Raman spectra are generally assigned to stretch vibration of T-O^o bonds (T

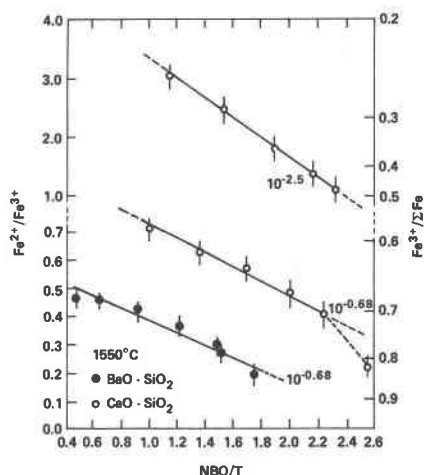


Fig. 3. Comparison of relations between Fe²⁺/Fe³⁺ and NBO/T for melts on the joins CaO-SiO₂ and BaO-SiO₂ with 5 wt.% Fe₂O₃ added and equilibrated at 1550°C in air and for CaO-SiO₂ also at f_{O₂} = 10^{-2.5}. In these compositions, the NBO/T was calculated with Fe³⁺ as a network former, as discussed further in text.

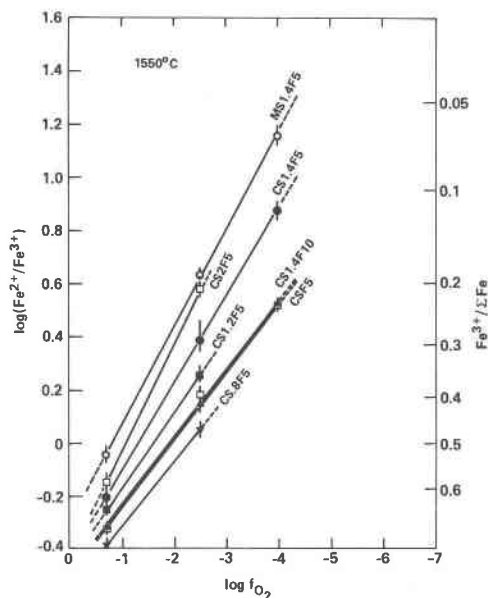


Fig. 4. Log (Fe²⁺/Fe³⁺) vs. log *f*_{O₂} for melts equilibrated at 1550°C as a function of melt composition, type of metal cation and amount of iron added. For the expression, log (Fe²⁺/Fe³⁺) = *a* log *f*_{O₂} + *b*, the coefficients *a* and *b* are, respectively, CS2F5, -0.35 and -0.38; CS1.4F5, -0.33 and -0.42; CS1.4F10, -0.26 and -0.48; MS1.4F5, -0.36 and -0.28; CS1.2F5, -0.28 and -0.43; CSF5, -0.26 and -0.49; CS.8F5, -0.24 and -0.55.

= tetrahedral cation) where T is probably predominantly Fe³⁺ (Fox et al., 1982). In some of the glasses where the Mössbauer spectra suggest that tetrahedrally-coordinated ferric iron is absent, there remains a 900 cm⁻¹ band (see Table 3). Most likely, this band results from the existence of Si₂O₇²⁻ units in the melts. Whether such units also exist in Fe³⁺(IV)-bearing samples cannot be ascertained. This interpretation is consistent with that of Virgo et al. (1981, 1983b) for spectra of quenched melts (glasses) in the system Na₂O–SiO₂–Fe₂O₃–FeO where Fe³⁺ is in tetrahedral coordination. The values of IS_{Fe³⁺} and QS_{Fe³⁺} (Fig. 5, Table 1) from the Mössbauer spectra of these samples are similar to those found for tetrahedrally coordinated Fe³⁺ in crystalline ferrisilicates (Annersten and Halenius, 1976; Waychunas and Rossman, 1983; Amthauer et al., 1977). Thus, both the Mössbauer and the Raman data from the melts equilibrated in air at 1550°C are consistent with tetrahedrally coordinated ferric iron. The small but significant differences in IS_{Fe³⁺} and QS_{Fe³⁺} for tetrahedrally coordinated ferric iron with different cations for electric charge-balance (Table 2) may result from slightly different Fe³⁺–O distances in the tetrahedra and possibly some changes in polyhedral distortion.

The hyperfine parameters for ferric iron of quenched melts with Fe³⁺/ΣFe less than 0.5 (corresponding to log *f*_{O₂} = -2.5 at 1550°C) change rapidly from IS_{Fe³⁺} ~ 0.3 mm/sec and QS_{Fe³⁺} ~ 1.1 mm/sec at Fe³⁺/ΣFe ≥ 0.5 to IS_{Fe³⁺} ≥ 0.5 mm/sec and QS_{Fe³⁺} ≈ 0.8 mm/sec at Fe³⁺/

ΣFe ~ 0.4 or less (Fig. 5; Table 1). These changes in IS_{Fe³⁺} with decreasing Fe³⁺/ΣFe, as well as the temperature dependence of the hyperfine parameters for ferric iron obtained from spectra taken at 298 and 77 K with the respective low and high values of Fe³⁺/ΣFe (see Virgo et al., 1982, 1983a), are consistent with octahedrally coordinated ferric iron with Fe³⁺/ΣFe ≤ 0.4 and with tetrahedrally coordinated ferric iron with Fe³⁺/ΣFe ≥ 0.5. In the Fe³⁺/ΣFe range between 0.5 and 0.4, the Mössbauer data are consistent with a transition from tetrahedral to octahedral ferric iron where the two types of Fe³⁺–O polyhedra may coexist (see also Virgo et al., 1983a, for further discussion of the Mössbauer spectra of silicate melts with coexisting tetrahedral and octahedral ferric iron). Additional support for this interpretation of the Mössbauer data is the observation that the 900- and 990-cm⁻¹ depolarized Fe–O° symmetric stretch bands (generally assigned to Fe³⁺–O° in tetrahedral complexes; see also Fox et al., 1982) diminish in intensity with decreasing *f*_{O₂} (and decreasing Fe³⁺/ΣFe; Table 3, Fig. 6; see also footnote in Table 3 relating to ambiguities in this interpretation), thus also indicating the disappearance of Fe³⁺(IV)–O bonds in the melts as the Fe³⁺/ΣFe decreases.

The two ferrous doublets (e.g., Fig. 1; Table 1) differ in QS_{Fe²⁺} by more than 10%, with insignificant differences in IS_{Fe²⁺}. Such differences in quadrupole splitting for the two Fe²⁺–O octahedra may be related to their degree of distortion (Annersten and Olesch, 1978; Mysen and Virgo, 1978; Calas and Petiau, 1983; Waychunas and Rossman, 1983). With this interpretation, the Fe²⁺(II)–O polyhedron is the most distorted of the two.

Interaction between anionic units and ferric and ferrous iron

Some of the structural changes from Fe²⁺/Fe³⁺ variations and coordination transformation of Fe³⁺ in the melts may be evaluated with the Raman spectroscopic data (Fig. 6; Table 3). In the spectra, the relative abundance of anionic units is reflected in the relative intensities of the Raman bands that result from T–O bonds (T = tetrahedrally coordinated cation) in these units. Seifert et al. (1981) (see also Mysen et al., 1982a) devised a method by which the relative abundance of anionic units in individual MO–SiO₂ or M₂O–SiO₂ (M = a specific univalent or divalent metal cation) may be calculated as a function of M/Si of each system. This same method is used here for the system CaO–SiO₂–Fe–O. Results of these calculations are shown for composition CS1.4F5 as a function of its Fe³⁺/ΣFe (Fig. 7). In Figure 7 the relative abundance of tetrahedral Fe³⁺ units is omitted because of their low abundance. For the melt equilibrated in air at 1550°C, approximately 1.0% of the tetrahedral structure consists of Fe³⁺(IV)–O polyhedra. For lower values of Fe³⁺/ΣFe, Fe³⁺ is a network modifier, and the anionic network can be described entirely in terms of silicate units.

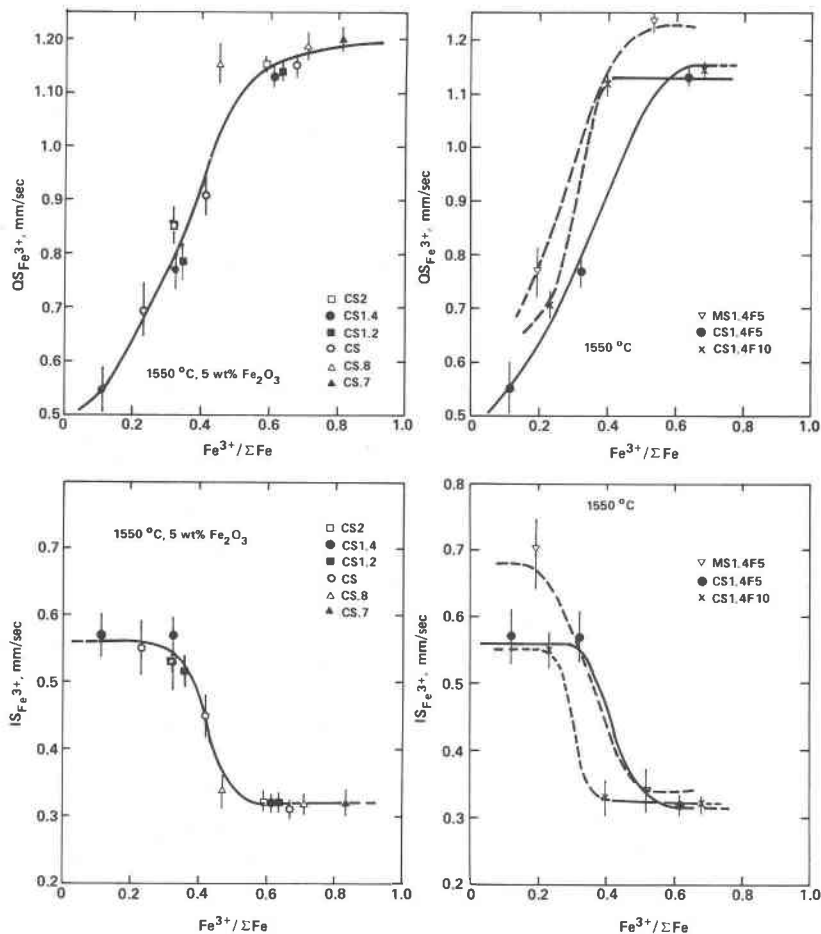
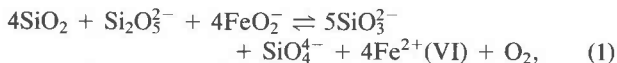


Fig. 5. Variations in hyperfine parameters for ferric iron (isomer shifts relative to Fe metal) ($IS_{Fe^{3+}}$ and $QS_{Fe^{3+}}$) as a function of $Fe^{3+}/\Sigma Fe$ along the join CaO–SiO₂, as a function of type of metal cation (Ca^{2+} and Mg^{2+}) and iron content.

There are several features of the data in Figure 7 indicating that Fe^{3+} and Fe^{2+} show different structural behavior than Si^{4+} and Ca^{2+} in melts in the system CaO–SiO₂–Fe–O. (Compare Fig. 3 in Mysen et al., 1982b, in which composition SW40 is equivalent to CS1.4 in the present study.) The composition CS1.4F5 at $f_{O_2} = 10^{-0.68}$ (air) and 1550°C has NBO/T = 1.36. Compared with melts with the same NBO/Si on the join CaO–SiO₂, the iron-bearing melt has a larger proportion of three-dimensional network units, less $Si_2O_5^{2-}$, less SiO_3^{2-} and slightly more SiO_4^{4-} . The increase in relative abundance of three-dimensional network units follows from the increased polymerization of composition CS1.4F5 compared with iron-free CS1.4 caused by tetrahedrally coordinated Fe^{3+} . This increase in SiO_2 units, coupled with an increase in SiO_3^{2-} and a decrease in $Si_2O_5^{2-}$, can also be related to the structural position of Fe^{2+} . The increase in the proportion of SiO_3^{2-} units indicates that Fe^{2+} –O polyhedra are formed with nonbridging oxygens from SiO_3^{2-} units rather than from nonbridging oxygens from $Si_2O_5^{2-}$. At constant NBO/Si, the $SiO_2 + SiO_3^{2-}$ increases

relative to $Si_2O_5^{2-}$ with increasing electronegativity of the metal cation (Liebau, 1981; Mysen et al., 1982b). Additional reduction of ferric to ferrous iron has only a very small effect on the overall degree of polymerization.

Inasmuch as $Fe(IV)^{3+}$ –O polyhedra appear to be three-dimensionally interconnected (Fox et al., 1982; Virgo et al., 1982, 1983b), this polyhedron may be described as FeO_2^- , as also suggested elsewhere (Paul and Douglas, 1965; Douglas et al., 1965; Goldman, 1983). One may then express a more complete redox equilibrium involving the silicate anionic structure, ferrous and ferric iron,



with the equilibrium constant

$$K_1 = \left(\frac{Fe^{2+(VI)}}{FeO_2^-} \right)^4 \left(\frac{SiO_3^{2-}}{SiO_2} \right)^4 \left(\frac{SiO_4^{4-} - SiO_3^{2-}}{Si_2O_5^{2-}} \right) f_{O_2}. \quad (2)$$

This expression is also consistent with the relationships between Fe^{2+}/Fe^{3+} , oxygen fugacity, NBO/T of the melt and Z/r^2 of the network-modifying cations (Figs. 2–4). In

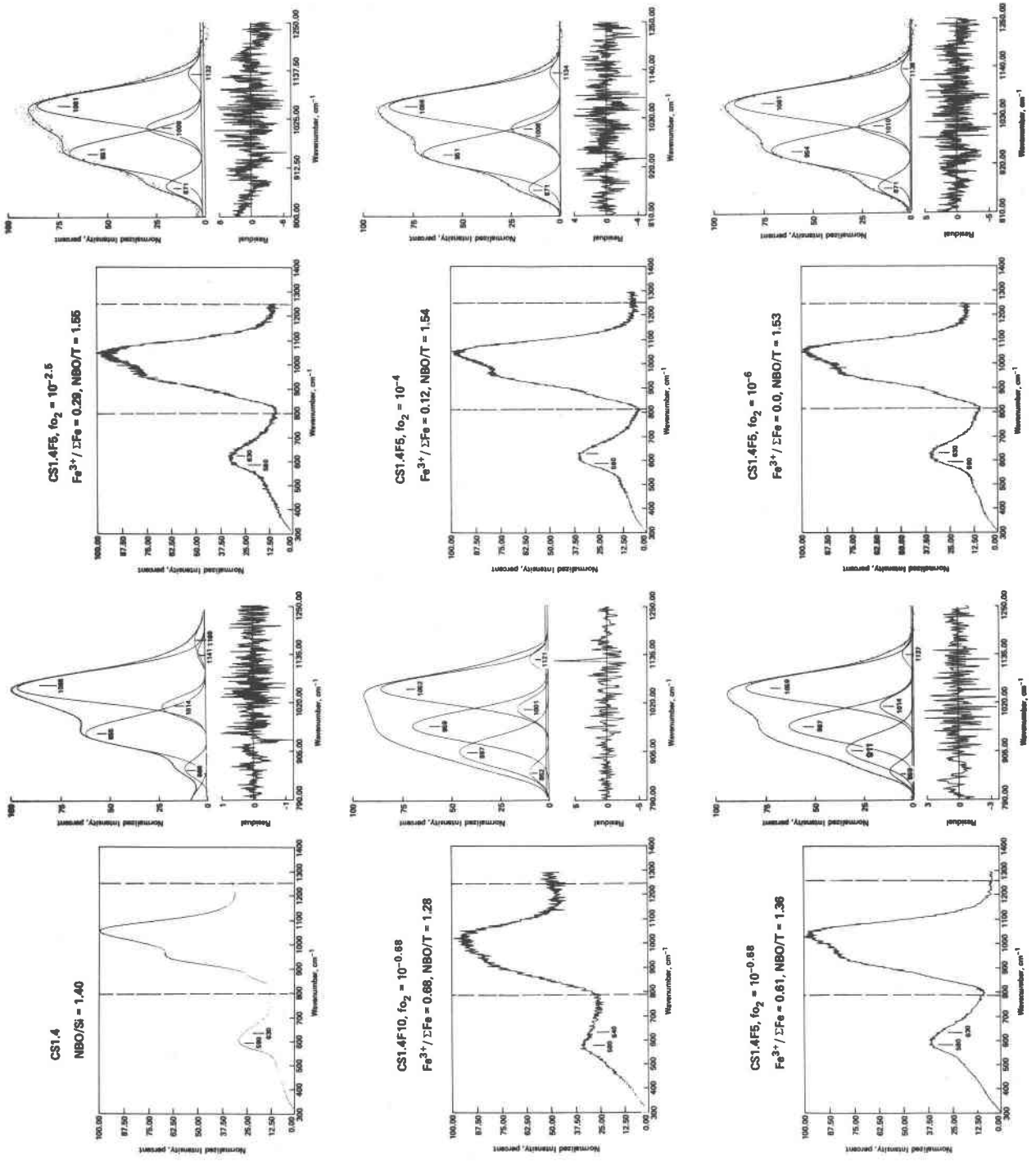


Fig. 6. Effect of oxygen fugacity ($Fe^{3+}/\Sigma Fe$) on the normalized and unpolarized Raman spectra of compositions CS1.4F5 and CS1.4F10 at 1550°C.

Table 3. Summary of relative areas (intensities) of Raman bands and their assignments

$-\log f_{O_2}$	Relative areas*					$Fe^{3+}/\Sigma Fe$	
	850†	900	950	1100	1150		
...	3.0	...	CS2	44.2	45.2	7.6	...
0.68	CS2F5	38.3	45.3	16.9	0.58
...	4.0	...	CS1.4	36.6	55.8	3.6	...
0.68	4.5	...	CS1.4F5	40.4	53.2	1.8	0.61
2.5	6.5	...		41.1	50.8	2.0	0.29
4.0	5.6	...		41.8	51.0	1.6	0.12
6.0	5.5	...		41.5	51.5	1.4	0.00
0.68	3.0	...	CS1.4F10	42.8	51.2	3.0	0.68
...	31.7	14.8	CS.8	53.2	0.3
0.68	30.8	27.9†	CS.8F5	41.3	...	0.71	...

*Areas are relative (%) to total integrated area of Si-O stretch bands in the 800-1200 cm^{-1} frequency range. In this high-frequency envelope, the intensities of the band near 1050 cm^{-1} ($Si-O^+$ stretch from bridging oxygen, e.g., Lasaga, 1982) and $Fe-O^+$ stretch bands (900 and 990 cm^{-1}) are excluded.

†850, etc., denote relative areas (intensities) of bands ($Si-O^-$ stretch in units of SiO_4^{4-} , $Si_2O_7^{6-}$, SiO_3^{2-} and $Si_2O_5^{2-}$ type, respectively) of Raman bands with frequencies approximated by these numbers. The 1150 represent the relative area of the $Si-O^+$ stretch from three-dimensional network units.

‡This intensity probably also includes a contribution from an unresolved $Fe-O^+$ stretch band near 900 cm^{-1} .

the range of bulk melt compositions of the present study, increasing NBO/T of the melt results in an increase in the relative abundance of SiO_3^{2-} and SiO_4^{4-} units and a decrease in SiO_2 and $Si_2O_5^{2-}$ (Furukawa et al., 1981; Mysen et al., 1982b). The relative increase in SiO_4^{4-} is

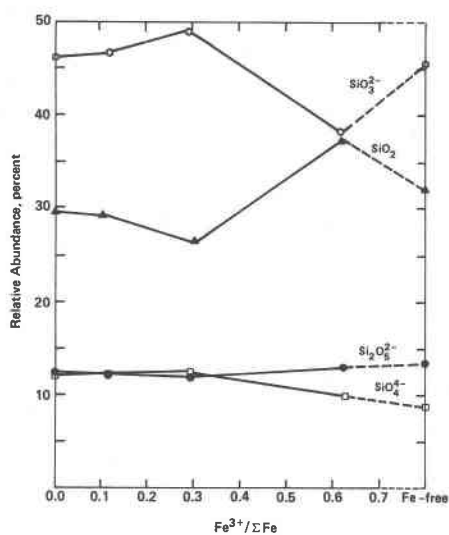


Fig. 7. Relative abundance of coexisting anionic units (recalculated to 100%; FeO_2^- units \approx 1%) as a function of $Fe^{3+}/\Sigma Fe$ for composition CS1.4F5. "Fe-free" denotes the relative abundances for the iron-free end member (compare also with SW40; Mysen et al., 1982b).

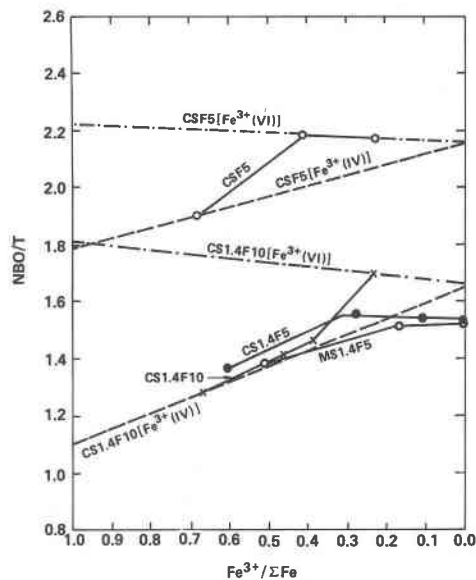


Fig. 8. Calculated degree of polymerization (NBO/T) of melts with 5 and 10 wt.% Fe_2O_3 added as a function of their $Fe^{3+}/\Sigma Fe$. Compositions CS1.4 and CS have $SiO_2/CaO = 1.4$ and 1.0, respectively, and MS1.4 has $SiO_2/MgO = 1.4$. F5 and F10 denote 5 and 10 wt.% Fe_2O_3 added to the starting material. The NBO/T is calculated from $Fe^{3+}/\Sigma Fe$ (Table 1) after structural assignment of Fe^{3+} . The lines CSF5 [$Fe^{3+}(VI)$], CSF5 [$Fe^{3+}(IV)$], CS1.4F5 [$Fe^{3+}(VI)$] and CS1.4 [$Fe^{3+}(IV)$] are calculated examples of the change in bulk melt NBO/T of these compositions as a function of $Fe^{3+}/\Sigma Fe$ if Fe^{3+} is a network modifier or a network former, respectively, over the entire $Fe^{3+}/\Sigma Fe$ range from 1.0 to 0.0.

small compared with that of SiO_3^{2-} . At constant f_{O_2} , the $(SiO_3^{2-}/SiO_2)^4 (SiO_3^{2-}SiO_4^{4-}/Si_2O_5^{2-})$ therefore increases. For constant K_1 this increase requires that $Fe^{2+}(VI)/FeO_2^-$ decrease. Thus, decreasing melt polymerization results in oxidation of ferrous to ferric iron as observed here (Fig. 4) and elsewhere (e.g., Douglas et al., 1965; Larson and Chipman, 1953).

Increasing Z/r^2 of the metal cation is positively correlated with Fe^{2+}/Fe^{3+} (Fig. 2; see also Douglas et al., 1965; Paul and Douglas, 1965; Mysen et al., 1980). This correlation may be understood by considering equations (1) and (2) together with the influence of different metal cations on the proportions of coexisting anionic units. Increasing Z/r^2 results in an increase in the abundance $(SiO_2 + SiO_3^{2-})$ relative to $Si_2O_5^{2-}$ units for melts with similar metal/silicon (Mysen et al., 1982b; see also Liebau, 1981). As a result of this abundance change, the ratio product $(SiO_3^{2-}/SiO_2)^4 (SiO_4^{4-}SiO_3^{2-}/Si_2O_5^{2-})$ in equation (2) is positively correlated with increasing Z/r^2 of the metal cation. In order to maintain the value of K_1 in equation (2), the Fe^{2+}/Fe^{3+} must decrease, in accord with observation.

Redox equilibria, melt structure and properties

Redox equilibria and melt polymerization

The redox ratio of iron oxides and the structural positions of Fe^{3+} and Fe^{2+} affect the overall degree of

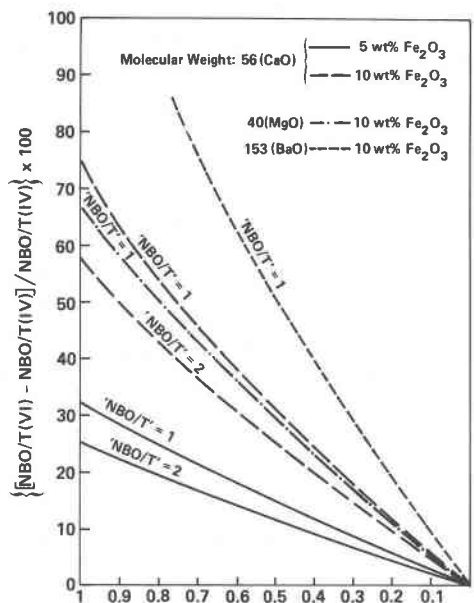


Fig. 9. Relative increase (%) in NBO/T of iron-bearing melts with network-modifying Fe^{3+} $[NBO/T(VI)]$ compared with the calculated NBO/T of the melt if Fe^{3+} is a network former $[NBO/T(IV)]$ as a function of total amount of iron, $Fe^{3+}/\Sigma Fe$, molecular weight of the metal oxide and degree of polymerization of the iron-free end member ("NBO/T").

polymerization of silicate melts (NBO/T). The NBO/T of several calcium silicate and magnesium silicate melts have been calculated as a function of their iron contents and $Fe^{3+}/\Sigma Fe$ (Fig. 8). For all compositions, the addition of 5 wt.% Fe_2O_3 or more to the starting materials results in polymerization relative to the iron-free end members because ferric iron is tetrahedrally coordinated in samples equilibrated with air at 1550°C. Under all conditions ferrous iron is in octahedral coordination (Mao et al., 1973; Bell and Mao, 1974; Nolet et al., 1979; Seifert et al., 1979; Mysen et al., 1980).

In Figure 8 the observed changes in NBO/T are compared with the hypothetical and calculated variations of NBO/T with Fe^{3+} as a network modifier $[Fe^{3+}(VI)]$ and network former $[Fe^{3+}(IV)]$ throughout the $Fe^{3+}/\Sigma Fe$ range from 1.0 to 0.0. Because Fe^{3+} undergoes a coordination transformation with $Fe^{3+}/\Sigma Fe < 0.5$, there is an initial continuous increase in NBO/T with decreasing $Fe^{3+}/\Sigma Fe$ and then a rapid change as Fe^{3+} is transformed to octahedral coordination (Fig. 8). There is thus a large difference in the degree of polymerization of iron-bearing silicate melts depending on $Fe^{3+}/\Sigma Fe$ and on whether Fe^{3+} is in tetrahedral coordination as illustrated with the calculated results shown in Figure 9. The extent of this difference is greater the smaller the NBO/T, the greater the total iron content and the larger the molecular weight of the metal cation.

Phase equilibria

In binary metal oxide-silica systems the degree of polymerization of liquidus minerals can be correlated

with the polymerization of the melt (see, e.g., Greig, 1927; Phillips and Muan, 1959, for relevant phase-equilibrium data on alkaline earth silicate systems). Such simple correlations no longer hold when Si^{4+} is replaced with a charge-balanced M^{3+} cation such as Fe^{3+} (or Al^{3+}) as indicated in Figure 10. In this figure the bulk melt NBO/T of the tridymite-pseudowollastonite liquidus boundary has been calculated for the system $CaO-FeO-Fe_2O_3-SiO_2$ (Osborn and Muan, 1960a) and compared with the melt compositions (expressed as NBO/T) for the same liquidus boundary in the system $CaO-Al_2O_3-SiO_2$ (Osborn and Muan, 1960b). The liquidus phase relations in the system $CaO-FeO-Fe_2O_3-SiO_2$ (Osborn and Muan, 1960a) were determined in equilibrium with air, where the temperatures along the tridymite-pseudowollastonite boundary increase from 1204°C at the invariant point tridymite + pseudowollastonite + hematite + liquid to 1436°C on the binary join $CaO-SiO_2$. Thus, the $Fe^{3+}/\Sigma Fe$ of the melts is less than 1. The redox ratios of iron used to compute the NBO/T of the melts on the liquidus boundary shown in Figure 10 were calculated from the present data (Table 2, Fig. 8). For all compositions, except perhaps those within 1-2 wt.% iron oxide, the ferric iron is tetrahedrally coordinated.

In view of the commonly observed correlation between liquidus phase equilibria and important features of the melt structure (see, e.g., Kushiro, 1975; Burnham, 1981; Fraser et al., 1983), the expansion of the pseudowollastonite liquidus volume to more polymerized compositions with increasing $M^{3+}/(M^{3+} + Si^{4+})$ ($M^{3+} = Al^{3+}$ or Fe^{3+}) indicates different structural roles of the tetrahedrally coordinated Fe^{3+} and Al^{3+} compared with that of Si^{4+} . A

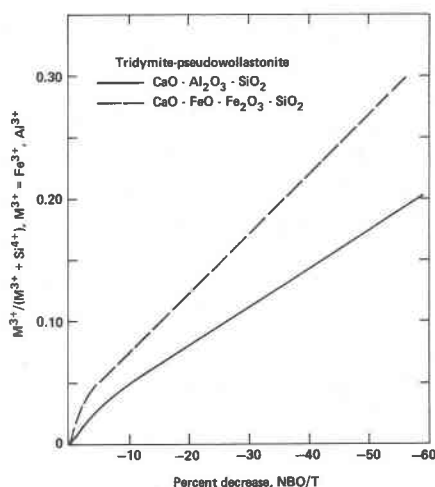


Fig. 10. Change (%) of degree of polymerization of liquids at the pseudowollastonite-tridymite liquidus boundary in the systems $CaO-Al_2O_3-SiO_2$ and $CaO-FeO-Fe_2O_3-SiO_2$ as a function of $M^{3+}/(M^{3+} + Si^{4+})$ of the liquid (M^{3+} refers to Fe^{3+} and Al^{3+}). The change is relative to the composition of the liquidus boundary in the system $CaO-SiO_2$. Phase-equilibrium data are from Osborn and Muan (1960a,b).

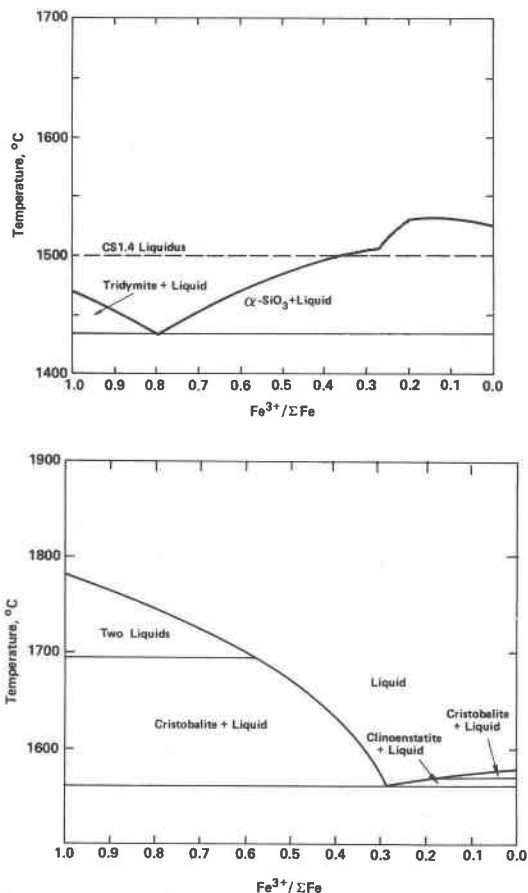


Fig. 11. Calculated liquidus phase equilibria of compositions CS1.4F10 and MS1.4F10 as a function of $\text{Fe}^{3+}/\Sigma\text{Fe}$.

simple polymerization by increasing $\text{Si}^{4+}/\text{Ca}^{2+}$ results in a contraction of the tridymite liquidus volume.

It can be seen (Fig. 10) that the liquidus volume of pseudowollastonite has expanded by slightly more than 50% (decrease in NBO/T of the melt relative to the value at the CaO-SiO_2 join) by the time hematite replaces the metasilicate liquidus phase. This expansion indicates that the activity of SiO_3^{2-} units in the melts has increased. The situation is similar in the system $\text{CaO-Al}_2\text{O}_3\text{-SiO}_2$ (Fig. 10). Thus, one may infer similar structural roles of Al^{3+} and Fe^{3+} with Ca^{2+} for charge-balance. Available Raman data indicate that both Al^{3+} (Mysen et al., 1981, 1982c) and Fe^{3+} (Fig. 6; see also Table 3 and Virgo et al., 1981, 1982) occur principally in three-dimensional network structural units in the melts. Solution of Fe_2O_3 (or Al_2O_3), therefore, tends to enhance the abundance of such units. This tendency requires, however, an increased abundance of depolymerized structural units in order to maintain mass balance, as illustrated by the schematic expression



In this expression, M could be either Fe^{3+} or Al^{3+} with suitable charge-balance for their tetrahedral coordination

together with Si^{4+} . Available data indicate that expressions such as (3) are shifted strongly to the right, thus leading to an enhanced proportion of three-dimensional network units together with depolymerized silicate units such as SiO_3^{2-} . With the assumption of ideal mixing of the M-cations in the MO_2 unit, the activity of SiO_2 will increase at a slower rate than that of SiO_3^{2-} because of the selective substitution of Al^{3+} and Fe^{3+} (or both) for Si^{4+} in the MO_2 units in the melts. As a result, increasing $\text{M}^{3+}/(\text{M}^{3+} + \text{Si}^{4+})$ ($\text{M}^{3+} = \text{Al}^{3+}$ or Fe^{3+}) causes an expansion of the liquidus volume of depolymerized silicate minerals.

Because the melt structure depends on $\text{Fe}^{3+}/\Sigma\text{Fe}$, liquidus phase equilibria of iron-free silicate minerals can be shown to vary with variable redox ratio of iron. Some consequences of these relationships can be pursued with calculated phase equilibria in portions of the systems $\text{CaO-SiO}_2\text{-Fe}_2\text{O}_3\text{-FeO}$ and $\text{MgO-SiO}_2\text{-Fe}_2\text{O}_3\text{-FeO}$ (Fig. 11). In Figure 11 the liquidus phase equilibria of compositions CS1.4 and MS1.4 (iron-free NBO/Si is 1.4 for both Ca- and Mg-bearing compositions) with 10 wt.% Fe_2O_3 added have been estimated as a function of $\text{Fe}^{3+}/\Sigma\text{Fe}$. The values of $\text{Fe}^{3+}/\Sigma\text{Fe}$ are, of course, simple functions of oxygen fugacity (see Fig. 4). Thus, oxygen fugacity could replace $\text{Fe}^{3+}/\Sigma\text{Fe}$ as the x axis in both figures. The calculated topologies of the phase diagrams depend solely on the chosen $\text{Fe}^{3+}/\Sigma\text{Fe}$ and the coordination polyhedra of Fe^{3+} and Fe^{2+} in the melts. The data reported above support these conclusions, but the liquidus phase equilibria shown in Figure 11 can be calculated without that information.

The phase equilibria have been obtained by calculating CaO/SiO_2 and MgO/SiO_2 of iron-free melts with NBO/Si corresponding to the NBO/T values obtained from the various values of $\text{Fe}^{3+}/\Sigma\text{Fe}$ and the structural position of Fe^{3+} in the melts. In these calculations, it is assumed, therefore, that $\text{Fe}^{3+}(\text{IV})$ occurs in separate complexes whose composition is not affected by the extensive and intensive variables. The abundance of these complexes merely affects the Si/O of the silicate network. It is also assumed that iron oxide minerals or solid solution of iron in the liquidus minerals is negligible, as indicated by the available phase-equilibrium data on the systems $\text{CaO-SiO}_2\text{-Fe-O}$ and $\text{MgO-SiO}_2\text{-Fe-O}$ (Muan and Osborn, 1965). Finally, it is assumed that the indicated preference of $\text{Fe}^{2+}(\text{VI})$ for SiO_3^{2-} and $\text{Fe}^{3+}(\text{VI})$ for SiO_4^{4-} units (see above) does not greatly affect the liquidus equilibria in the iron-concentration ranges of interest. For $\text{Fe}^{2+}(\text{VI})$, this assumption is probably justified for the Mg-bearing system in view of the crystal-chemical similarities of Fe^{2+} and Mg^{2+} . For the Ca-bearing system, the assumption probably leads to an underestimation of the activity of SiO_3^{2-} units. Thus, it is possible that the compositional range calculated as the liquidus stability field of metasilicate ($\alpha\text{-CaSiO}_3$) may be too narrow.

Octahedrally coordinated Fe^{3+} enhances the SiO_4^{4-} abundance in melts compared with both MgO-SiO_2 and CaO-SiO_2 . The maximum $\text{Fe}^{3+}/(\text{M}^{2+} + \text{Fe}^{3+})$ is, however, so small (0.049 at $\text{Fe}^{3+}/\Sigma\text{Fe} = 0.3$ in CS1.4F10) that a

possible affinity of Fe^{3+} for specific anionic units such as SiO_4^{4-} has a negligible effect on the activities of other units in the melt. Inasmuch as the units of particular interest are meta- and tectosilicates, the neglect of the Fe^{3+} (VI) association with SiO_4^{4-} is justified.

In the system CaO-SiO_2 (Phillips and Muan, 1959), the melt polymerization (decrease in NBO/Si) resulting from addition of 10 wt.% Fe_2O_3 results in a change from pseudowollastonite at 1500°C to tridymite on the liquidus at 1470°C (Fig. 11). The tridymite liquidus field extends to $\text{Fe}^{3+}/\Sigma\text{Fe} \sim 0.8$ at the minimum liquidus temperature in the system ($\sim 1435^\circ\text{C}$). Additional reduction of ferric to ferrous iron is associated with pseudowollastonite on the liquidus and an increase in liquidus temperatures. These phase equilibria result from the increased liquidus temperature along the join CaO-SiO_2 in the Ca/Si range (or $\text{NBO/Si} = 2\text{Ca/Si}$) corresponding to the increased NBO/Si resulting from decreasing $\text{Fe}^{3+}/\Sigma\text{Fe}$. A maximum liquidus temperature occurs between $\text{Fe}^{3+}/\Sigma\text{Fe} = 0.2$ and 0.1 .

With less than 10 wt.% Fe_2O_3 added to CS1.4 composition, reduction of ferric to ferrous iron may not result in a sufficient NBO/Si increase (to 1.7) to reach the thermal maximum. For end-member CaO-SiO_2 compositions with higher Ca/Si than that of CS1.4, the maximum liquidus temperature occurs with higher values of $\text{Fe}^{3+}/\Sigma\text{Fe}$, or for the same $\text{Fe}^{3+}/\Sigma\text{Fe}$, with lower total iron contents. Finally, there is a narrow $\text{Fe}^{3+}/\Sigma\text{Fe}$ range with discontinuous changes in the slope of the pseudowollastonite liquidus curve. This $\text{Fe}^{3+}/\Sigma\text{Fe}$ range corresponds to that where Fe^{3+} undergoes transformation from network former to network modifier. For lower iron contents, this behavior of the liquidus curves will occur at higher $\text{Fe}^{3+}/\Sigma\text{Fe}$ (higher oxygen fugacity).

The composition MS1.4 has the same M/Si (and, therefore, similar NBO/Si in the molten form) in the system MgO-SiO_2 as CS1.4 in the system CaO-SiO_2 . The phase equilibria in MgO-SiO_2 are, however, considerably different from those of CaO-SiO_2 (Greig, 1927; Phillips and Muan, 1959). First, MS1.4 has cristobalite on the liquidus, whereas the liquidus phase of the CS1.4 composition is a metasilicate (pseudowollastonite). This difference transcends into the system $\text{MgO-SiO}_2\text{-Fe}_2\text{O}_3\text{-FeO}$ (Muan and Osborn, 1956; see also Muan and Osborn, 1965, for summaries of relevant phase-equilibrium data). In equilibrium with air, MS1.4 + 10 wt.% Fe_2O_3 (MS1.4F10) has two immiscible liquids coexisting at 1780°C , whereas for CS1.4F10, tridymite is a liquidus phase at 1470°C . In the magnesium-bearing system, as in the calcium-bearing system, decreasing $\text{Fe}^{3+}/\Sigma\text{Fe}$ (decreasing f_{O_2}) results in a rapid calculated decrease in the liquidus temperature to a minimum near 1570°C for $\text{Fe}^{3+}/\Sigma\text{Fe} \sim 0.3$ where cristobalite coexists with clinoenstatite (Fig. 11). The coexisting tectosilicate and metasilicate at the temperature minimum were also observed for CS1.4F10 but at higher values of $\text{Fe}^{3+}/\Sigma\text{Fe}$ (~ 0.8). Furthermore, the lowering of the liquidus temperature by reduction of ferric to ferrous iron is much greater in the system $\text{MgO-SiO}_2\text{-Fe}_2\text{O}_3\text{-FeO}$ ($\sim 200^\circ\text{C}$) than in the sys-

tem $\text{CaO-SiO}_2\text{-Fe}_2\text{O}_3\text{-FeO}$ ($\sim 35^\circ\text{C}$). For the MS1.4F10 composition, a further decrease in $\text{Fe}^{3+}/\Sigma\text{Fe}$ results in a temperature increase along which liquidus clinoenstatite remains over only a narrow composition interval before cristobalite again becomes a liquidus phase. This trend differs from that of CS1.4F10, where the metasilicate liquidus mineral remains until $\text{Fe}^{3+}/\Sigma\text{Fe} = 0$ (Fig. 11).

Summary

From the Raman and Mössbauer spectroscopic data coupled with published phase equilibria it is concluded that:

1. The Fe^{3+} is tetrahedrally coordinated in silicate melts with alkaline earths for charge-balance and $\text{Fe}^{3+}/\Sigma\text{Fe} > 0.4\text{--}0.5$, whereas for melts with lower $\text{Fe}^{3+}/\Sigma\text{Fe}$, ferric iron is a network modifier. Ferrous iron is always a network modifier.

2. The polymerization (NBO/T) of silicate melts is a function of $\text{Fe}^{3+}/\Sigma\text{Fe}$. All melt properties that depend on NBO/T are therefore dependent on $\text{Fe}^{3+}/\Sigma\text{Fe}$.

3. The $\text{Fe}^{3+}/\Sigma\text{Fe}$ of alkaline earth silicate melts has simple functional relations to oxygen fugacity, temperature and the type of alkaline earth metal. Thus, the NBO/T of the melts depend on the same intensive and extensive variables.

4. Liquidus volumes of iron-free silicate minerals (e.g., meta- and tectosilicate minerals) can then be estimated as a function of iron contents and $\text{Fe}^{3+}/\Sigma\text{Fe}$ of the liquid.

Acknowledgments

Critical reviews by L. W. Finger, P. McMillan, E. F. Osborn and H. S. Yoder, Jr., are appreciated.

References

- Amthauer, G., Annersten, H., and Hafner, S. S. (1977) The Mössbauer spectrum of ^{57}Fe in titanium-bearing andradites. *Physics and Chemistry of Minerals*, 1, 399-413.
- Annersten, H. and Halenius, U. (1976) Ion distribution in pink muscovite: a discussion. *American Mineralogist*, 61, 1045-1050.
- Annersten, H. and Olesch, M. (1978) Distribution of ferrous and ferric iron in clintonite and the Mössbauer characteristics of ferric iron in tetrahedral coordination. *Canadian Mineralogist*, 18, 199-204.
- Bell, P. M. and Mao, H. K. (1974) Crystal-field spectra of Fe^{2+} and Fe^{3+} in synthetic basalt glass as a function of oxygen fugacity. *Carnegie Institution of Washington Year Book*, 73, 496-497.
- Bowen, N. L., Schairer, J. F., and Willems, H. W. V. (1930) The ternary system: $\text{Na}_2\text{SiO}_3\text{-Fe}_2\text{O}_3\text{-SiO}_2$. *American Journal of Science*, 20, 405-455.
- Brawer, S. A. and White, W. B. (1977) Raman spectroscopic investigation of the structure of silicate glasses. II. Soda-alkaline earth-alumina ternary and quaternary glasses. *Journal of Non-Crystalline Solids*, 23, 261-278.
- Burnham, C. W. (1981) The nature of multicomponent aluminosilicate melts. *Physics and Chemistry of the Earth*, 13-14, 197-227.
- Calas, G. and Petiau, J. (1983) Structure of oxide glasses:

- spectroscopic studies of local order and crystallochemistry: geochemical implications. *Bulletin de Minéralogie*, 106, 33–55.
- Chou, I.-M. (1978) Calibration of oxygen buffers at high *P* and *T* using the hydrogen fugacity sensor. *American Mineralogist*, 63, 690–703.
- Deines, P., Nafziger, R. H., Ulmer, G. C., and Woermann, E. (1974) Temperature-oxygen fugacity tables for selected gas mixtures in the system C–H–O at one atmosphere total pressure. *Bulletin of the Earth and Mineral Sciences, Pennsylvania State University*, 88.
- Dickinson, M. P., and Hess, P. C. (1981) Redox equilibria and the structural role of iron in aluminosilicate melts. *Contributions to Mineralogy and Petrology*, 78, 352–358.
- Domine, F. and Periou, B. (1983) Study of sodium silicate melts and glasses with infrared reflectance spectroscopy. *Journal of Non-Crystalline Solids*, 55, 125–131.
- Douglas, E. W., North, P., and Paul, A. (1965) Oxygen ion activity and its influence on the redox equilibrium in glasses. *Physics and Chemistry of Glasses*, 6, 216–233.
- Eibschutz, M. and Lines, M. E. (1982) Observation of second-order quadrupole shift in Mössbauer spectrum of amorphous YAG (yttrium garnet). *Physical Reviews B*, 25, 4256–4259.
- Eibschutz, M., Lines, M. E., and Nassau, K. (1980) Electric field-gradient distribution in vitreous yttrium garnet. *Physical Review B*, 21, 3767–3770.
- Fox, K. E., Furukawa, T., and White, W. B. (1982) Transition metal ions in silicate melts. Part 2. Iron in sodium silicate glasses. *Physics and Chemistry of Glasses*, 23, 169–178.
- Fraser, D. G., Rammensee, W., and Jones, R. H. (1983) The mixing properties of melts in the system $\text{NaAlSi}_2\text{O}_6$ – KAlSi_2O_6 determined by Knudsen cell mass spectrometry. *Bulletin de Minéralogie*, 106, 111–117.
- Fudali, F. (1965) Oxygen fugacity of basaltic and andesitic magmas. *Geochimica et Cosmochimica Acta*, 29, 1063–1075.
- Furukawa, T., Fox, K. E., and White, W. B. (1981) Raman spectroscopic investigation of the structure of silicate glasses. III. Raman intensities and structural units in sodium silicate glasses. *Journal of Chemical Physics*, 75, 3226–3237.
- Goldman, D. S. (1983) Oxidation equilibrium of iron in borosilicate glass. *Journal of the American Ceramic Society*, 66, 205–209.
- Greig, J. W. (1927) Immiscibility in silicate melts, Pt. II. *American Journal of Science*, 13, 133–155.
- Haggerty, S. E. (1978) The redox state of planetary basalts. *Geophysical Research Letters*, 5, 443–446.
- Kushiro, I. (1975) On the nature of silicate melt and its significance in magma genesis: regularities in the shift of liquidus boundaries involving olivine, pyroxene and silica minerals. *American Journal of Science*, 275, 411–431.
- Larson, H. and Chipman, J. (1953) Oxygen activity in iron oxide slags. *Transactions of the American Institute of Mining and Metallurgical Engineers*, 196, 1089–1096.
- Lasaga, A. C. (1982) Optimization of CNDO for molecular orbital calculation on silicates. *Physics and Chemistry of Minerals*, 8, 36–46.
- Lauer, H. V. and Morris, R. V. (1977) Redox equilibria of multivalent ions in silicate melts. *Journal of the American Ceramic Society*, 60, 443–451.
- Levitz, P., Bonnin, D., Calas, G., and Legrand, A. P. (1980) A two-parameter distribution analysis of Mössbauer spectra in non-crystalline solids using general inversion method. *Journal of Physics E: Scientific Instruments*, 13, 427–437.
- Liebau, F. (1981) The influence of cation properties on the conformation of silicate and phosphate anions. In A. Navrotsky and M. O'Keeffe, Eds., *Structure and Bonding in Crystals*, Vol. 2, p. 197–232. Academic Press, New York.
- Mao, H. K., Virgo, D., and Bell, P. M. (1973) Analytical study of the orange lunar soil returned by the Apollo 17 astronauts. *Carnegie Institution of Washington Year Book*, 72, 631–638.
- Muan, A. and Osborn, E. F. (1956) Phase equilibria at liquidus temperatures in the system MgO – FeO – Fe_2O_3 – SiO_2 . *Journal of the American Ceramic Society*, 39, 121–140.
- Muan, A. and Osborn, E. F. (1965) Phase Equilibria Among Oxides in Steelmaking. Addison-Wesley, Reading, Massachusetts.
- Mysen, B. O. and Virgo, D. (1978) Influence of pressure, temperature and bulk composition on melt structures in the system $\text{NaAlSi}_2\text{O}_6$ – $\text{NaFe}^{3+}\text{Si}_2\text{O}_6$. *American Journal of Science*, 278, 1307–1322.
- Mysen, B. O., Seifert, F. A., and Virgo, D. (1980) Structure and redox equilibria of iron-bearing silicate melts. *American Mineralogist*, 65, 867–884.
- Mysen, B. O., Virgo, D., and Kushiro, I. (1981) The structural role of aluminum in silicate melts—a Raman spectroscopic study at 1 atmosphere. *American Mineralogist*, 66, 678–701.
- Mysen, B. O., Finger, L. W., Seifert, F. A., and Virgo, D. (1982a) Curve-fitting of Raman spectra of amorphous materials. *American Mineralogist*, 67, 686–696.
- Mysen, B. O., Virgo, D., and Seifert, F. A. (1982b) The structure of silicate melts: implications for chemical and physical properties of natural magma. *Reviews of Geophysics*, 20, 353–383.
- Mysen, B. O., Virgo, D., and Seifert, F. A. (1982c) Distribution of aluminum between anionic units in depolymerized silicate melts as a function of pressure and temperature. *Carnegie Institution of Washington Year Book*, 81, 360–366.
- Navrotsky, A., Peraudeau, P., McMillan, P., and Coutoures, J.-P. (1982) A thermochemical study of glasses and crystals along the joins silica-calcium aluminate and silica-sodium aluminate. *Geochimica et Cosmochimica Acta*, 46, 2039–2049.
- Nolet, D. A., Burns, R. G., Flamm, S. L., and Besancon, J. R. (1979) Spectra of Fe-Ti silicates: implications to remote sensing of planetary surfaces. *Proceedings of the 10th Lunar and Planetary Science Conference*, 1775–1786.
- Osborn, E. F. and Muan, A. (1960a) Phase equilibrium diagrams of oxide systems. Plate 10. The system CaO –“ Fe_2O_3 ”– SiO_2 . American Ceramic Society, Columbus, Ohio.
- Osborn, E. F. and Muan, A. (1960b) Phase equilibrium diagrams of oxide systems. Plate 2. The system CaO – Al_2O_3 – SiO_2 . American Ceramic Society, Columbus, Ohio.
- Paul, A. and Douglas, R. W. (1965) Ferrous-ferric equilibrium in binary alkali silicate glasses. *Physics and Chemistry of Glasses*, 6, 207–211.
- Phillips, B. and Muan, A. (1959) Phase equilibria in the system CaO –iron oxide– SiO_2 in air. *Journal of the American Ceramic Society*, 42, 413–423.
- Presnall, D. C. and Brenner, N. L. (1974) A method for studying iron silicate liquids under reducing conditions with negligible iron loss. *Geochimica et Cosmochimica Acta*, 38, 1785–1788.
- Sato, M. (1972) Electrochemical measurements and control of oxygen fugacity and other gaseous fugacities with solid electrolyte systems. In G. C. Ulmer, Ed., *Research Techniques for High Pressure and High Temperature*, p. 43–99. Springer Verlag, New York.
- Sato, M. and Valenza, M. (1980) Oxygen fugacities of the

- layered series of the Skaergaard intrusion, East Greenland, *American Journal of Science*, 280-A, 134–158.
- Seifert, F. A., Virgo, D., and Mysen, B. O. (1979) Melt structures and the redox equilibria in the system $\text{Na}_2\text{O}-\text{FeO}-\text{Fe}_2\text{O}_3-\text{Al}_2\text{O}_3-\text{SiO}_2$. *Carnegie Institution of Washington Year Book*, 78, 511–519.
- Seifert, F. A., Mysen, B. O., and Virgo, D. (1981) Quantitative determination of proportions of anionic units in silicate melts. *Carnegie Institution of Washington Year Book*, 80, 301–302.
- Seifert, F. A., Mysen, B. O., and Virgo, D. (1982) Three-dimensional network melt structure in the systems $\text{SiO}_2-\text{NaAlO}_2$, $\text{SiO}_2-\text{CaAl}_2\text{O}_4$ and $\text{SiO}_2-\text{MgAl}_2\text{O}_4$. *American Mineralogist*, 67, 696–718.
- Verweij, H. (1979a) Raman study of the structure of alkali germanosilicate glasses. I. Sodium and potassium metagermanosilicate glasses. *Journal of Non-Crystalline Solids*, 33, 41–53.
- Verweij, H. (1979b) Raman study of the structure of alkali germanosilicate glasses. II. Lithium, sodium and potassium digermanosilicate glasses. *Journal of Non-Crystalline Solids*, 33, 55–69.
- Verweij, H. and Konijnendijk, W. L. (1976) Structural units in $\text{K}_2\text{O}-\text{PbO}-\text{SiO}_2$ glasses by Raman spectroscopy. *Journal of the American Ceramic Society*, 59, 517–521.
- Virgo, D., Mysen, B. O., and Kushiro, I. (1980) Anionic constitution of silicate melts quenched at 1 atm from Raman spectroscopy: implications for the structure of igneous melts. *Science*, 208, 1371–1373.
- Virgo, D., Mysen, B. O., and Seifert, F. A. (1981) Relationship between the oxidation state of iron and structure of silicate melts. *Carnegie Institution of Washington Year Book*, 80, 308–311.
- Virgo, D., Mysen, B. O., Danckwerth, P. A., and Seifert, F. A. (1982) Speciation of Fe^{3+} in 1-atm $\text{Na}_2\text{O}-\text{SiO}_2-\text{Fe}-\text{O}$ melts. *Carnegie Institution of Washington Year Book*, 81, 349–353.
- Virgo, D., Mysen, B. O., and Danckwerth, P. A. (1983a) The coordination of Fe^{3+} in oxidized vs. reduced sodium aluminosilicate glasses: a ^{57}Fe Mössbauer study. *Carnegie Institution of Washington Year Book*, 82, 309–313.
- Virgo, D., Mysen, B. O., and Danckwerth, P. A. (1983b) Redox equilibria and the anionic structure of $\text{Na}_2\text{O} \cdot x\text{SiO}_2-\text{Fe}-\text{O}$ melts: effects of oxygen fugacity. *Carnegie Institution of Washington Year Book*, 82, 305–309.
- Waychunas, G. A. and Rossman, G. R. (1983) Spectroscopic standard for tetrahedrally coordinated ferric-iron: $\gamma\text{LiAlO}_2:\text{Fe}^{3+}$. *Physics and Chemistry of Minerals*, 9, 212–215.
- Whittaker, E. J. W. and Muntus, R. (1970) Ionic radii for use in geochemistry. *Geochimica et Cosmochimica Acta*, 34, 945–957.
- Wivel, C. and Morup, S. (1981) Improved computational procedure for evaluation of overlapping hyperfine parameter distributions in Mössbauer spectra. *Journal of Physics E: Scientific Instruments*, 14, 605–610.

*Manuscript received, October 21, 1983;
accepted for publication, May 1, 1984.*